Hsp70 biases the folding pathways of client proteins

Ashok Sekhar[a,b,c,1], Rina Rosenzweig[a,b,c,d,1], Guillaume Bouvignies[e,f,g], and Lewis E. Kay[a,b,c,h,2]

[a]Department of Molecular Genetics, The University of Toronto, Toronto, ON, Canada M5S 1A8; [b]Department of Biochemistry, The University of Toronto, Toronto, ON, Canada M5S 1A8; [c]Department of Chemistry, The University of Toronto, Toronto, ON, Canada M5S 1A8; [d]Department of Structural Biology, Weizmann Institute of Science, Rehovot 76100, Israel; [e]Département de Chimie, École Normale Supérieure (ENS)-Paris Sciences et Lettres (PSL) Research University, 75005 Paris, France; [f]Laboratoire des Biomolécules (LBM), Sorbonnes Universités, Université Pierre et Marie Curie (UPMC), Université Paris 06, 75005 Paris, France; [g]UMR 7203 LBM, CNRS, 75005 Paris, France; and [h]Program in Molecular Structure and Function, Hospital for Sick Children, Toronto, ON, Canada M5G 1X8

Edited by G. Marius Clore, National Institutes of Health, Bethesda, MD, and approved March 23, 2016 (received for review February 2, 2016)

The 70-kDa heat shock protein (Hsp70) family of chaperones bind cognate substrates to perform a variety of different processes that are integral to cellular homeostasis. Although detailed structural information is available on the chaperone, the structural features of folding competent substrates in the bound form have not been well characterized. Here we use paramagnetic relaxation enhancement (PRE) NMR spectroscopy to probe the existence of long-range interactions in one such folding competent substrate, human telomere repeat binding factor (hTRF1), which is bound to DnaK in a globally unfolded conformation. We show that DnaK binding modifies the energy landscape of the substrate by removing long-range interactions that are otherwise present in the unbound, unfolded conformation of hTRF1. Because the unfolded state of hTRF1 is only marginally populated and transiently formed, it is inaccessible to standard NMR approaches. We therefore developed a ^{1}H-based CEST experiment that allows measurement of PREs in sparse states, reporting on transiently sampled conformations. Our results suggest that DnaK binding can significantly bias the folding pathway of client substrates such that secondary structure forms first, followed by the development of longer-range contacts between more distal parts of the protein.

Hsp70 | protein folding | excited states | molecular chaperones | PRE

The 70-kDa heat shock protein (Hsp70) chaperone system is an important component of the cellular proteostasis machinery, serving as a central hub to channel client proteins along folding, refolding, maturation, disaggregation, and proteolytic pathways in cooperation with other chaperone assemblies such as Hsp90, Hsp104, and GroEL/ES (1–3). Central to Hsp70 function is its ATP-dependent interaction with client proteins, facilitated by Hsp40 cochaperones and nucleotide exchange factors (NEFs) (4). Hsp70 is a weak ATPase that recognizes and binds substrates at sites containing large aliphatic hydrophobic residues, Ile, Leu, and Val, flanked by positively charged amino acids such as Arg and Lys (5). Initial binding of substrate to the ATP-form of Hsp70 can occur directly, or via Hsp40, with rapid on/off kinetics that give rise to a weak overall affinity for the interaction. Subsequent ATP hydrolysis, stimulated by interactions with Hsp40 and substrate, leads to a large conformational change in the chaperone, locking the substrate in the Hsp70 bound state. The resulting complex is of high affinity with slow substrate on/off rates (2).

Escherichia coli DnaK is the best studied of Hsp70 chaperones. It is a 70-kDa protein comprised of an N-terminal ATPase and a C-terminal substrate binding domain that communicate allosterically to couple ATP hydrolysis with substrate binding (3). High-resolution structures of ADP- (6) and ATP-DnaK (7, 8) establish that these two domains dock on to one another in the ATP-DnaK state, but become detached from each other in the ADP-bound form. In contrast to the detailed structural studies characterizing DnaK, little atomic resolution data are available on the conformation of folding-competent client proteins in the DnaK-bound state. It is known that DnaK binds substrates in a globally unfolded conformation with varying degrees of local residual native and nonnative secondary structure (9–13). However, whether stable or transient long-range interactions are present in DnaK-bound client proteins remains an open question that has relevance for understanding the function of DnaK in substrate refolding and disaggregation. For example, it has been shown that DnaK, in concert with cochaperones DnaJ (Hsp40) and GrpE (NEF), converts misfolded luciferase to a globally unfolded, yet folding-competent, conformation (14). Furthermore, the DnaK chaperone system is thought to "loosen" aggregated proteins for subsequent disaggregation by ClpB or proteolysis by ClpXP (15). Aggregated and misfolded proteins are stabilized by native and nonnative tertiary contacts and characterizing the extent to which these interactions either persist or are modified upon DnaK binding will provide insights into the mechanism by which DnaK carries out its myriad of important functions.

Here we probe the existence of (transient) long-range tertiary interactions in a folding competent substrate, the human telomere repeat binding factor (hTRF1), which is globally unfolded when bound to DnaK (13), using paramagnetic relaxation enhancement (PRE) NMR spectroscopy. To evaluate whether DnaK binding modifies the energy landscape of the substrate in a way that affects long-range interactions in the unfolded state, we have recorded PREs in the unbound, unfolded conformation of hTRF1 under identical conditions to those used for studies of DnaK-bound hTRF1. The unfolded state of hTRF1 in water (referred to in what follows as uw-hTRF1) is only sparsely populated and transiently formed, rendering it invisible to standard NMR studies. However,

Significance

Hsp70 (70-kDa heat shock protein) chaperones bind cognate substrates to prevent their aggregation and guide them toward their correctly folded, functional states. Here we use NMR spectroscopy to understand how this is achieved by studying a complex of Hsp70 with a folding competent substrate. Using an NMR experiment presented here, we show that long-range transient contacts are established in the unfolded, unbound state of the substrate. These contacts are greatly attenuated in the bound form of the substrate that also exists as an unfolded ensemble. Our results establish that Hsp70 binding can significantly bias the folding mechanism of client substrate molecules toward pathways where secondary structure is first generated, followed by the establishment of longer-range interactions in a distance-dependent fashion.

Author contributions: A.S., R.R., and L.E.K. designed research; A.S., R.R., and L.E.K. performed research; G.B. contributed new reagents/analytic tools; A.S., R.R., and L.E.K. analyzed data; and A.S., R.R., and L.E.K. wrote the paper.

The authors declare no conflict of interest.

This article is a PNAS Direct Submission.

Data deposition: The NMR chemical shifts for K52C-hTRF1 in 3.5 M urea have been deposited in the Biological Magnetic Resonance Bank (BMRB), www.bmrb.wisc.edu (accession no. 26764).

[1]A.S. and R.R. contributed equally to this work.

[2]To whom correspondence should be addressed. Email: kay@pound.med.utoronto.ca.

This article contains supporting information online at www.pnas.org/lookup/suppl/doi:10.1073/pnas.1601846113/-/DCSupplemental.

Downloaded from https://www.pnas.org by UNIVERSITY OF MASSACHUSETTS on May 18, 2022 from IP address 128.119.52.1.

the signal from the invisible state can be amplified using chemical exchange saturation transfer (CEST) and read out through the visible, folded hTRF1 state. We thus developed a ^{1}H-based CEST experiment that facilitates measurement of PREs in uw-hTRF1. A comparison of PREs in this state with those in the hTRF1-DnaK bound conformation establishes that the large PREs in uw-hTRF1 are significantly reduced on DnaK binding, and the extent of residual long-range interactions in the DnaK-bound form is similar to hTRF1 denatured in 4 M urea. Taken together, our results suggest that DnaK may be able to modify the folding pathways of protein substrates by significantly influencing their tertiary structural tendencies in the bound conformation.

Results

Measuring Long-Range Interactions in Unfolded and DnaK-Bound hTRF1. The human telomerase repeat binding factor is a 53-residue three-helix bundle belonging to the homeodomain family of proteins (Fig. 1*A*) (16, 17). Native hTRF1 has a predicted DnaK binding site (5) centered at Leu-30 in helix 2 (Fig. 1*A*, blue) and binds ADP-DnaK with a K_D of 32 μM (35 °C) in a manner that is very similar to the well-characterized DnaK-binding peptide from the *E. coli* heat shock transcription factor σ^{32} (13). Interestingly, DnaK-bound hTRF1 is globally unfolded but retains as much as 40% helicity in regions forming helices 1 and 3 in the native protein, which are distal to the DnaK binding site (13). hTRF1 is marginally stable and the folded conformer of the WT protein interconverts with an unfolded state with a fractional population of ∼4% and with a lifetime on the order of 3 ms (35 °C), $G \underset{k_{EG}}{\overset{k_{GE}}{\rightleftharpoons}} E$, where the ground ($G$) and excited ($E$) states refer to the native and uw-hTRF1 states, respectively, and k_{lm} is the rate constant for the conversion from l to m (13). Although NMR cross-peaks from the uw-hTRF1 state cannot be observed, its chemical shifts could be recorded (13) using CEST-based experiments (18–20). These experiments have been developed for characterizing conformationally exchanging states that interconvert on the order of or less than several hundreds per second with excited state populations of ∼1% or higher (18). A comparison of the secondary structural propensities of DnaK-bound hTRF1 with those of the unfolded state revealed similar patterns of helicity in both states, showing that DnaK binding does not prevent the formation of secondary structure in the bound substrate protein (13).

Having established that the innate secondary structural propensities of the cognate hTRF1 substrate are retained on binding to DnaK we now wish to probe longer-range interactions. In particular, we wish to investigate whether DnaK binding, leading to a globally unfolded ensemble of hTRF1 conformers, modifies residual tertiary contacts, both nonnative and native-like, that may be present in unbound, uw-hTRF1. However, quantifying long-range interactions in uw-hTRF1 is not straightforward because spectra of this state cannot be directly recorded, and although CEST-based experiments have proven powerful for obtaining chemical shifts of excited states, these shifts are much more sensitive to secondary structure and contain little information on tertiary contacts (21). Indeed, the lack of NMR approaches for obtaining long-range structural constraints in invisible states has posed a significant limitation in the characterization of these elusive conformers.

PREs, generated by attachment of a spin label to a reactive cysteine in a protein, are powerful structural constraints that have been used in a large number of structural studies of both folded (22, 23) and unfolded proteins (24–28) and to generate atomic models of molecular complexes (29, 30). The r^{-6} dependence of the PRE on the distance between the unpaired electron of the spin label and the affected NMR probe provides long range information that extends up to distances of 25–30 Å (31), significantly larger than those obtained from nuclear Overhauser effect (NOE) measurements. However, the PRE effect also scales as the square of the gyromagnetic ratio of the nuclear spin (γ) that is relaxed by the unpaired electron of the spin label, attenuating the effect for nuclei such as ^{13}C and ^{15}N that have γ values that are 0.25 and 0.10, respectively, of the ^{1}H nucleus. In what follows, therefore, the strategy is to measure ^{1}H PREs in the uw-hTRF1 excited state via a ^{1}H CEST experiment that is described below and compare such enhancements with those measured on a DnaK-bound hTRF1 complex, as illustrated schematically in Fig. 1*B*.

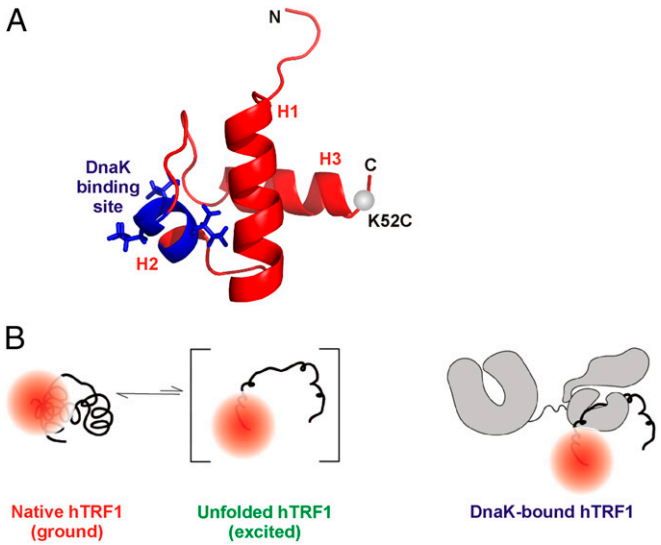

Fig. 1. Using PREs to compare long-range interactions in DnaK-bound and uw-hTRF1. (*A*) Cartoon representation of the structure of hTRF1 [Protein Data Bank (PDB) ID code 1BA5] (16). The DnaK binding site is highlighted in blue, and the sidechains of the ILL residues at its core are shown as sticks. The site of attachment of the nitroxide spin label (residue 52) is shown as a gray sphere. (*B*) PREs can be measured directly on DnaK-bound hTRF1 (*Right*), but not on uw-hTRF1 because it is a sparsely populated and transiently formed state that exchanges slowly with native (ground) hTRF1.

Measuring PREs in Slowly Exchanging Excited Protein States. Clore and coworkers (31) have shown that it is possible to obtain PREs of spins in the excited state directly from relaxation measurements of nuclei in the ground state of an interconverting system in cases where the exchange is fast, both on the chemical shift timescale and relative to the difference in transverse relaxation rates (R_2) of NMR spin probes in the ground (small PRE) and excited (large PRE) states (typically k_{ex} >> 10,000 s^{-1}). For hTRF1, where the exchange between native and unfolded conformers is ∼300 s^{-1} (35 °C), such an approach is thus not feasible. We have, therefore, developed a ^{1}H CEST-based method in which a weak ^{1}H radiofrequency B_1 field is applied at systematically varying ^{1}H frequencies, covering the complete range of possible amide proton resonance positions for a protein. In cases where exchange is two state, as for the unfolding reaction of hTRF1, the resulting peak intensity derived from a spin in the ground state has a B_1 frequency-dependent profile that shows major and minor dips, at the positions of the ground and excited state chemical shifts for the spin in question. Amplification of peak intensities from the invisible state is achieved by ^{1}H irradiation at the resonance positions of excited state nuclei and the subsequent transfer of this perturbation to the ground state spins by chemical exchange. The major and minor state dips for each nucleus are sensitive to the ^{1}H R_2s of the spins in each of their respective states, which can be obtained by fitting the CEST profiles to models of two-state exchange using the Bloch–McConnell equations (32) describing the evolution of exchanging

Downloaded from https://www.pnas.org by UNIVERSITY OF MASSACHUSETTS on May 18, 2022 from IP address 128.119.52.1.

magnetization under conditions of radiofrequency irradiation. Accordingly, per-residue ^{1}H R_2 values for excited state spins can, in principle, be obtained for a system in conformational exchange by recording CEST experiments using ^{1}H longitudinal magnetization. By repeating the experiment for samples where the spin label is oxidized (oxid) and reduced (red), PREs are calculated as the difference in fitted R_2 values according to $\Gamma_2^{NH} = R_2^{oxid} - R_2^{red}$.

There is, however, a complicating feature. When ^{1}H longitudinal magnetization is irradiated the change in intensity can be transferred between spins via chemical exchange, as described above, or alternatively by an NOE effect. In the latter case, the perturbation is propagated to proximal ^{1}H spins, resulting in dips in CEST profiles that are difficult to distinguish from chemical exchange (33). NOE dips are not a concern for applications that involve ^{15}N or ^{13}C CEST because the γ values of these spins are smaller than for ^{1}H, and hence the homonuclear dipolar effect that scales as γ^4 is, for all practical purposes, negligible. However, the effect is significant for ^{1}H CEST and requires a modification to the experimental approach. Thus, rather than focusing on longitudinal ^{1}H magnetization, we initially create ^{1}H-^{15}N two-spin order, $2I_zN_z$, where I_z and N_z denote z-magnetization from one-bond coupled ^{1}H and ^{15}N spins, respectively. Irradiation of the ^{1}H component of $2I_zN_z$ occurs during a mixing time, T_{EX}, and the perturbation to $2I_zN_z$ is subsequently read out using the pulse sequence of Fig. 2*A* (further details of the pulse scheme are presented in *SI Text*). CEST dips arise from chemical exchange in a similar way as in experiments that irradiate longitudinal magnetization because longitudinal order interconverts between states ($2I_z^GN_z^G \underset{k_{EG}}{\overset{k_{GE}}{\rightleftarrows}} 2I_z^EN_z^E$) in an analogous manner to longitudinal magnetization ($I_z^G \underset{k_{EG}}{\overset{k_{GE}}{\rightleftarrows}} I_z^E$). However, dipolar cross-relaxation between proximal protons, I and S, that leads to NOE dips in CEST profiles when I_z is allowed to evolve during T_{EX}, instead results in the creation of terms connecting ^{1}H and ^{15}N spins that are not scalar coupled, $2I_zN_z \rightarrow 2S_zN_z$. Importantly, at the start of CEST irradiation, longitudinal order of the form $2S_zN_z$ does not exist, whereas for CEST experiments that quantify the evolution of longitudinal magnetization during the CEST delay, both I_z and S_z can be approximately equally populated, depending on the exact details of the experiment (*SI Text*). This crucial difference in initial conditions between CEST experiments can lead to a significantly slower build-up of NOE dips when longitudinal order is evolved during T_{EX}, greatly simplifying analysis of the data. Additional discussion is presented in Fig. S1, where relative sizes of NOE dips in I_z- and $2I_zN_z$-based CEST experiments are compared, showing that even for small proteins, such as hTRFI, significant NOE dips can be obtained when longitudinal magnetization evolves during CEST, whereas NOE effects are very much minimized in the pulse scheme of Fig. 2*A*.

CEST-Based ^{1}H R_2 Measurements in uw-hTRF1. To obtain insight into long-range interactions in uw-hTRF1, as a basis for comparison with hTRF1 bound to DnaK, Lys-52 at the C-terminal end of helix 3 was mutated to Cys and a nitroxide-based tempol spin label attached to the Cys thiol group (Fig. 1*A*). The ^{1}H-^{15}N heteronuclear single quantum Coherence (HSQC) spectrum of reduced K52C-tempol hTRF1 is well resolved, characteristic of a folded protein (Fig. S2). Using the experiment described above (Fig. 2*A*), ^{1}H CEST profiles were recorded on oxidized and reduced samples of K52C-tempol hTRF1 using four different B_1 fields per sample ranging from 16 to 53 Hz, with an exchange duration (T_{EX}) of 125 ms. Representative ^{1}H CEST profiles of K52C-tempol hTRF1 in which the spin label is reduced (*Upper*) and oxidized (*Lower*) are shown in Fig. 2*B* and Fig. S3, with the major and minor dips at the resonance positions of the native ground state and the corresponding unfolded excited state for each spin, respectively. Each dip is further split by the one-bond ^{1}H-^{15}N scalar-coupling because ^{15}N decoupling is not applied during T_{EX} (*SI Text*), although for many residues the resulting doublet cannot be resolved. For peaks such as Leu-7 with a large PRE in the excited state, the width of the minor dip is distinctly broader in the oxidized sample than in the reduced one (Fig. 2*B*).

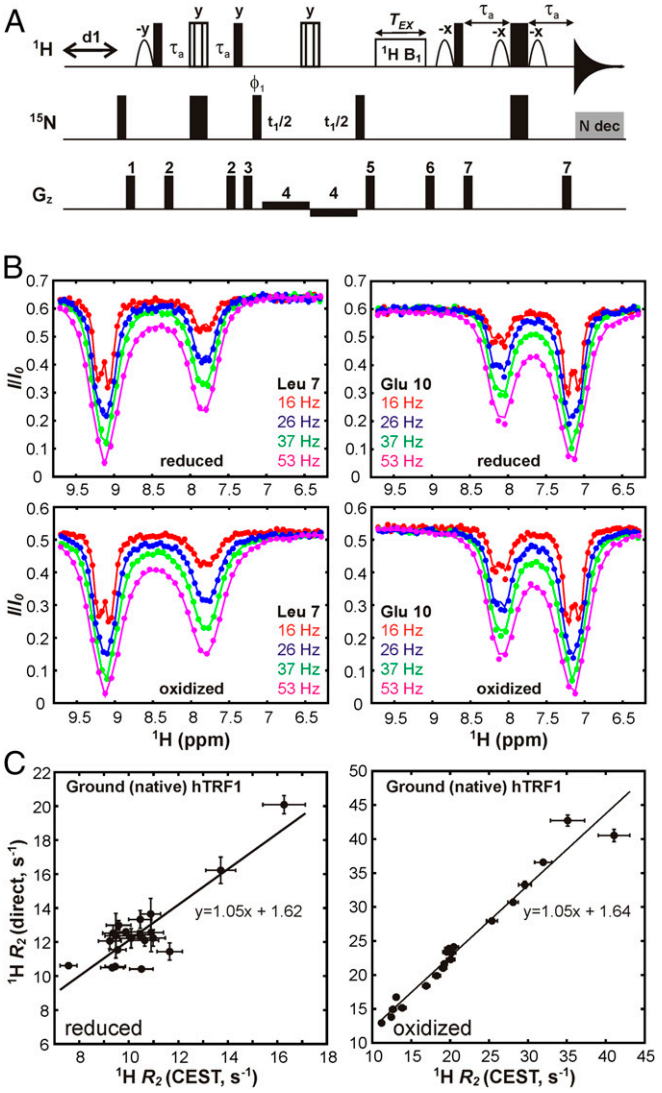

Fig. 2. ^{1}H CEST-based method for measuring PREs in excited protein states in slow conformational exchange with a ground state. (*A*) ^{1}H-CEST pulse scheme that has been used. Narrow and wide filled bars correspond to 90° and 180° pulses, respectively. Open shapes are water selective 90° pulses, whereas striped 180° pulses are of the composite variety (57), 90°$_x$-180°$_y$-90°$_x$. Central to the experiment is the delay T_{EX} during which a weak ^{1}H radio frequency field is applied to longitudinal order, ultimately generating the CEST profiles. Further details are given in *SI Text*. (*B*) Representative CEST profiles of L7 (*Left*) and E10 (*Right*) of uw-hTRF1 with the nitroxide spin label at position 52 in reduced (*Upper*) and oxidized (*Lower*) forms. Ratios of intensities of cross-peaks in the presence (I) and absence (I_o) of delay T_{EX} are plotted along the y axis as a function of the position of the weak ^{1}H B_1 field along x. (*C*) Correlation between ^{1}H CEST-derived and directly measured R_2 values of amide protons in the native (ground) state of hTRF1 when the spin-label is reduced (*Left*) or oxidized (*Right*). The equation for the best-fit line (solid line) is indicated on the plot.

^{1}H CEST profiles for residues with distinct major and minor dips ($|\Delta\varpi_{GE}| > 0.3$ ppm) were globally fit to a two-state model of chemical exchange as detailed in *SI Text* to extract populations and rates of interconversion between ground and excited states,

Downloaded from https://www.pnas.org by UNIVERSITY OF MASSACHUSETTS on May 18, 2022 from IP address 128.119.52.1.

as well as residue specific ^{1}H R_2 values for nuclei in G and E. The CEST experiment has the advantage of separating the interconverting conformers according to their chemical shifts, facilitating the extraction of state-specific R_2 values. Moreover, modeling the CEST profiles using the Bloch–McConnell equations that explicitly take into account the exchange between the major and minor conformers provides exchange-free measures of R_2. All of the CEST data could be well fit to a model of two-site exchange with χ^2_{red} values of 1.1 and 1.2 for the oxidized and reduced samples respectively, and $\Delta\varpi_{GE}$ values for the two samples match very well, implying that the excited state in both cases is the same (Fig. S4*B*). In addition, CEST-derived ^{15}N chemical shifts of K52C-tempol and WT hTRF1 obtained by fitting ^{15}N CEST data to two-state models of chemical exchange correlate very well to each other (Fig. S4*C*), confirming that the water unfolded states populated by both proteins are essentially identical.

Validating CEST-Derived ^{1}H R_2 Rates Measured in Ground and Excited States. As described above ^{1}H R_2 values for nuclei in each of the exchanging states can be obtained from fits of CEST profiles in the case where dips corresponding to the major and minor states are well resolved. Using a cutoff of $|\Delta\varpi_{GE}| > 0.3$ ppm and focusing on residues that could be analyzed in both oxidized and reduced states allowed us to obtain transverse relaxation rates for 20 amide protons in hTRF1 (Fig. 2*C* and Fig. S5). CEST-derived ^{1}H R_2 values for reduced hTRF1 in the ground state (native conformation) are small and spread over a narrow range spanning 10–16 s^{-1}, consistent with expectations for a small deuterated folded protein domain (Fig. S5*A*). ^{1}H R_2 rates for some amide spins in the reduced, excited state (uw-hTRF1) are larger than the corresponding values for the native conformation, with the difference likely arising from enhanced hydrogen exchange with solvent H_2O in the unprotected, unfolded state (Fig. S5*B*). Indeed, all uw-hTRF1 ^{1}H R_2 values are less than 20 s^{-1} for a reduced sample containing more Cl^-, as is expected because chloride ions suppress hydrogen exchange (34), and there are significant increases in ^{1}H R_2 rates of the uw-state when the pH is increased from 6 to 7. Residue-specific ^{1}H R_2 values measured for both native and unfolded hTRF1 in the oxidized sample are larger than the rates obtained for the reduced sample (Fig. S5 *C* and *D*), so that PREs are present in both ground and excited state conformers as discussed below. Although errors in CEST derived R_2 values are typically about 0.3–2 s^{-1} in the native ground state, they are considerably larger in the excited state (5–12 and 4–18 s^{-1} in reduced and oxidized samples, respectively; Figs. S5 and S6) so that care must be taken in interpreting small PRE values.

Because the methodology for measuring ^{1}H R_2 relaxation rates via CEST is new, it must be cross-validated. Validation can be achieved experimentally for the ground state by recording free-precession amide ^{1}H transverse relaxation rates (35) on oxidized and reduced hTRF1 samples directly and subsequently subtracting from the obtained rates the contribution from chemical exchange. Fig. 2*C* shows the linear correlation obtained between direct (y axis) and CEST-based (x axis) rates, and the agreement is relatively good between the two different measurements, indicating that robust ground state transverse relaxation rates can be obtained from fitting CEST profiles. There is a small slope of 5% and an offset of 1.6 s^{-1} between CEST and direct measurements of ^{1}H R_2 rates. As shown in *SI Text* (Fig. S7), extracted R_2 values from CEST are sensitive to B_1 miscalibration, and small errors on the order of 3–5% in the B_1 field can lead to the differences noted here between direct and CEST-based R_2 values.

R_2 values for nuclei in the excited state cannot be measured directly because correlations from such rare conformers are not observed in spectra. We have therefore evaluated the robustness of excited state R_2 rates via computations whereby 10 ^{1}H CEST profiles were simulated using parameter ranges determined from the experimental data and fit to a two-state model as detailed in *SI Text*. This procedure was repeated 500 times using different realizations of experimental noise added to the CEST data, and errors in output parameters were calculated on the basis of the distribution of the fitted values. Good correlations between input and fitted excited state R_2 values are obtained, establishing that at least for the case of our work on hTRF1, ^{1}H CEST experiments provide reliable estimates of transverse relaxation rates (Fig. S8 *A–C*). Small systematic deviations between input and output values broadly correlate inversely to $\Delta\varpi_{GE}$, emphasizing the importance of analyzing only CEST profiles for which major and minor dips are separated (Fig. S8 *D* and *E*). Simulations were also performed to establish that neglecting (*i*) cross-relaxation of proximal protons with the amide of interest, as well as (*ii*) cross-correlation between dipole-dipole and chemical shift anisotropy relaxation mechanisms in fitting of CEST profiles does not affect the robustness of extracted ground and excited state R_2 values under our experimental conditions (*SI Text* and Fig. S8 *F* and *G*).

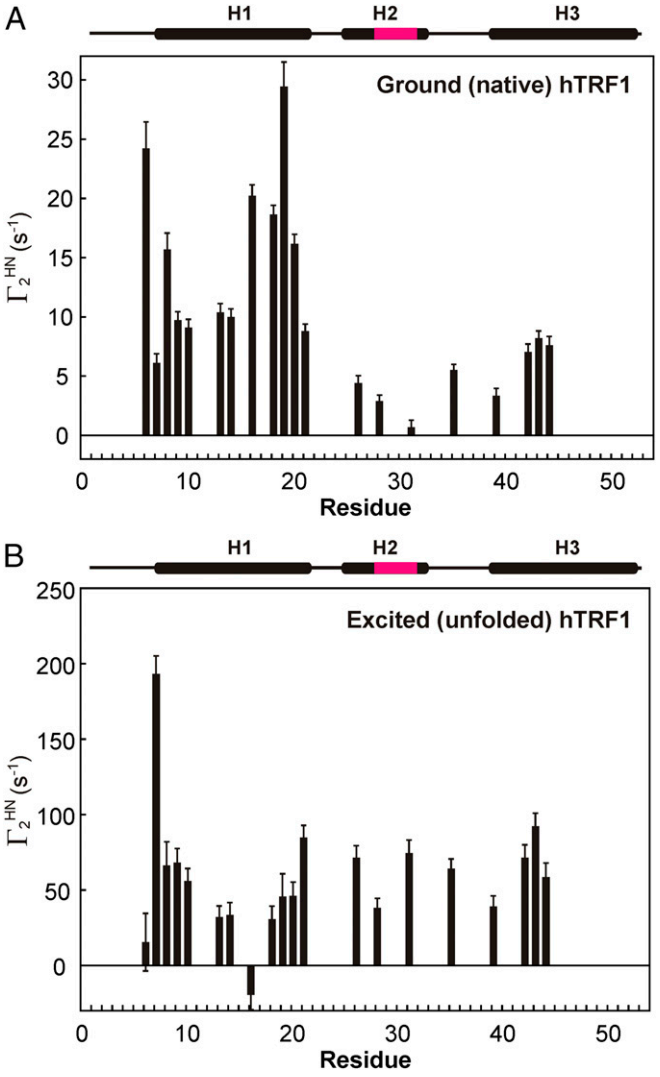

Fig. 3. Residue-specific PRE values of native (ground, *A*) and water unfolded (excited, *B*) hTRF1. The secondary structure of hTRF1 is shown above each plot and the DnaK binding site is indicated in magenta.

Downloaded from https://www.pnas.org by UNIVERSITY OF MASSACHUSETTS on May 18, 2022 from IP address 128.119.52.1.

PREs in uw-hTRF1. Residue-specific PREs of ground (native) and excited (unfolded) hTRF1 were calculated as the difference between R_2 rates obtained by fitting CEST profiles measured in oxidized and reduced samples and are plotted in Fig. 3. Helix 1 has the largest PREs in the native state (Fig. 3*A*), up to 28 s^{-1}, whereas distances between the amides of helix 2 and the spin label (position 52 in helix 3) are sufficiently large so that PRE values less than ∼5 s^{-1} are measured. The proximity of the spin label to many of the amides of helix 3 makes it difficult to quantify PREs in this region. Measured PRE values in the excited state are much larger overall (Fig. 3*B*), reflecting the greater flexibility of uw-hTRF1 and the lack of a rigid core structure that allows the spin label to come close to much of the protein. Notably, large PREs are observed for residues Leu-7–Lys-12 and Val-18–Tyr-21 in both folded and unfolded states, suggesting that helix 1–helix 3 interactions are also present in uw-hTRF1 (Fig. 3*B*). Interestingly, significant PREs (∼50–75 s^{-1}) are also seen in helix 2 of the unfolded ensemble but not in the native conformer, that are consistent with the presence of nonnative helix 2–helix 3 interactions in uw-hTRF1 (Fig. 3*B*). PREs in both native and unfolded states do not change systematically with concentration, confirming that they derive from intra- rather than intermolecular interactions (Fig. S5 *E* and *F*).

PREs in DnaK-Bound hTRF1. To determine whether long-range interactions are present in DnaK-bound hTRF1, samples containing 300 μM highly deuterated (^{2}H) ADP-DnaK and 140 μM ^{15}N/^{2}H-labeled K52C-tempol hTRF1 in the reduced and oxidized forms were prepared. ^{1}H-^{15}N HSQC spectra of these samples show that the bound substrate is globally unfolded, as was observed previously for WT hTRF1 in complex with ADP-DnaK (Fig. S9). Amide ^{1}H R_2 values for the reduced and oxidized samples were measured directly, with the PREs of the DnaK-bound form of hTRF1 shown in Fig. 4*A* (blue). Relaxation rates, and hence PRE values, could not be obtained for residues in helix 2, that contains the DnaK binding site, because cross-peaks were not observed in this region of the protein. Further, the few observable peaks from helix 3 could not be properly quantified because of their low intensity that results from the placement of the spin label at the end of this helix. A comparison with PRE values measured for uw-hTRF1 (Fig. 4*A*, green) establishes that DnaK binding significantly reduces the interactions present in the free form of the substrate. Although helix 2–helix 3 contacts are not expected to be present in the DnaK-bound state, because they are disrupted by the bound DnaK, it is clear that helix 1–helix 3 contacts are also very significantly diminished in the DnaK-bound complex.

PREs in Urea-Unfolded hTRF1. Our results clearly show that the long-range contacts in uw-hTRF1 are disrupted on DnaK binding; however, residual small PRE values in the DnaK-bound state in helix 1 do remain. Are PRE values of this magnitude representative of contacts that are made at random in a denatured protein? To address this we measured PREs in the urea-unfolded state of hTRF1 (uu-hTRF1; Fig. S10). Such conformers are in general more extended (36) with less residual secondary structure than compact, unfolded states in water (37). PREs in urea-unfolded K52C-tempol hTRF1, calculated from ^{1}H free precession R_2 measurements on oxidized and reduced samples, are shown in Fig. 4*A* (black). Small PRE values are measured for residues in helices 1 and 2 with slightly larger rates in helix 3 close to the spin label. Notably, PREs in helix 1 are comparable in magnitude for urea-unfolded and DnaK-bound hTRF1, suggesting that DnaK binding results in an extended unfolded state. In contrast, uu-hTRF1 contains little or no helicity in regions corresponding to helices 1–3 in the native structure (Fig. 4*B*), unlike both uw-hTRF1 and the DnaK-bound state. Taken together, our results indicate that the level of secondary structure of the DnaK-bound client protein is comparable to that in the unfolded state in the absence of denaturants, whereas the extent of transient tertiary contacts is similar to what is found in the urea denatured unfolded ensemble.

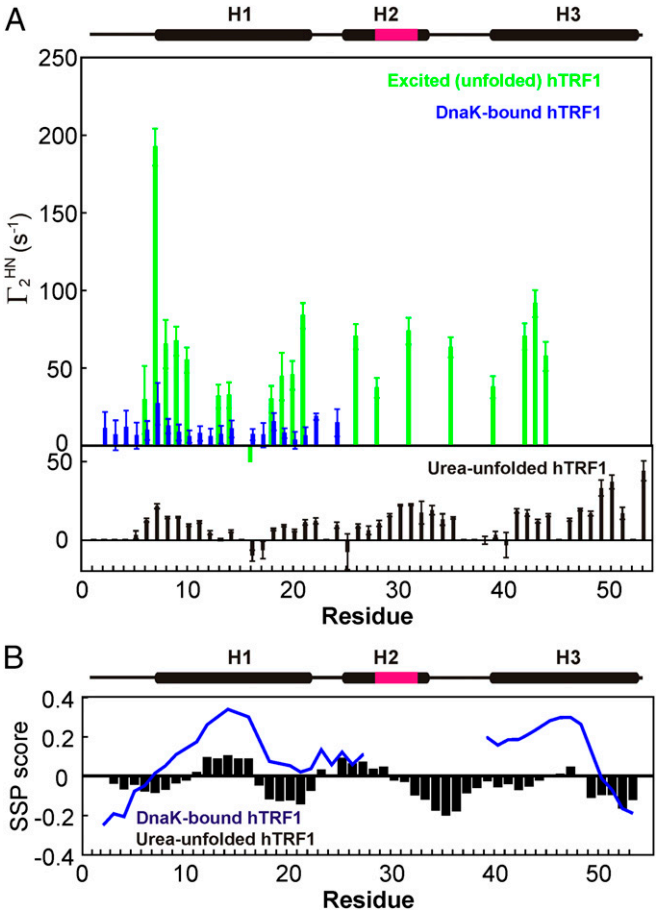

Fig. 4. Comparisons of long-range interactions within DnaK-bound hTRF1, uw-hTRF1, and uu-hTRF1. (*A*) PRE values in the DnaK-bound (blue), uw- (green), and uu- (black) states of hTRF1. (*B*) Secondary structural propensities (58) of DnaK-bound (blue) and uu- (black) hTRF1. In both panels, the secondary structure of hTRF1 is indicated above the plots with the DnaK-binding site denoted in magenta.

Discussion

Proteins are dynamic molecules that can access alternate energy conformations due to thermal fluctuations from the ground state (38, 39). Such rare conformers are likely of importance in folding, misfolding, and function. Recent advances in protein NMR spectroscopy, exploiting well-known methods such as Carr-Purcell-Meiboom-Gill (CPMG) (40–42) and $R_{1\rho}$ relaxation dispersion (43), as well as CEST (18, 44, 45), have led to the identification and structural characterization of invisible biomolecular conformers that are populated to greater than 0.5% and have lifetimes in excess of ∼100 μs (46). Structural information on such conformationally excited states is available in the form of chemical shifts (47) and chemical shift anisotropies (48), residual dipolar couplings (49, 50), and hydrogen exchange rates (51). However, long-range distance information has been difficult to obtain except for systems in very fast exchange (k_{ex} > 10,000 s^{-1}) (31). Here we introduce a method based on ^{1}H CEST for generating such distance information in the form of PREs for relatively slow exchanging systems (50–400 s^{-1}) that is therefore complementary to the corresponding methods for fast interconversion. Such PREs provide distances between an unpaired electron, typically a nitroxide spin label attached to an intrinsic Cys or one introduced at a

Downloaded from https://www.pnas.org by UNIVERSITY OF MASSACHUSETTS on May 18, 2022 from IP address 128.119.52.1.

specific position in the protein, and a proton nucleus. The distances so obtained, typically up to ~25–30 Å, can serve as valuable restraints for biomolecular structure calculations or for docking molecules in a complex. Because CEST experiments that exploit ^{1}H longitudinal magnetization are subject to complications from the generation of NOE dips that cannot be separated from those arising from chemical exchange, we developed an experiment based on longitudinal order that is less sensitive to such effects. For the exchange parameters germane to the system considered here, we established, through experiment and simulation, that reliable estimates of ground and excited state R_2 rates can be obtained, provided that major and minor CEST dips are sufficiently separated (on the order of ~0.3 ppm). Because decay rates of longitudinal order can be relatively fast in a protonated protein, typically on the order of the selective ^{1}H R_1 rates (52), recording experiments using samples that are deuterated at nonexchangeable proton positions is recommended. In addition to reducing cross-relaxation with external protons and hence decreasing relaxation rates so that slower exchange processes can be studied, deuteration also increases the signal-to-noise in experiments per unit measurement time. Moreover, by limiting the number of external proton spins, deuteration leads to a decrease in potential errors that are introduced using a model for data analysis that neglects interactions between multiple proton spins (*SI Text*). In this regard, it is noteworthy that simulations establish that placing an external proton 2.75 Å from the amide in question does not lead to errors in parameters extracted using a simplified model that does not take into account the additional spin (*SI Text*).

Here we address whether DnaK binding to a substrate can disrupt transient long-range interactions that would otherwise be present in the unbound protein. A new ^{1}H-based CEST experiment is developed to measure PREs in the sparsely populated water unfolded state of hTRF1 and the resultant PREs are compared with those obtained for DnaK-bound hTRF1. We have previously shown that hTRF1 binds DnaK in a globally unfolded conformation, possessing local residual secondary structure at a level comparable to that present in uw-hTRF1 (13). On the basis of the PRE data reported here we find that there are native-like helix 1–helix 3 and potentially nonnative helix 2–helix 3 interactions in uw-hTRF1 (Fig. 3*B*) which are broken or considerably weakened upon DnaK binding (Fig. 4*A*). The magnitude of PREs in urea-unfolded and DnaK-bound hTRF1 states are similar, suggesting that the DnaK-bound client protein is extended in a similar way to a urea-unfolded protein chain (Fig. 4*A*).

Our results demonstrate that DnaK binding disrupts long-range interactions while concomitantly allowing local structure to form in the associated client protein (Fig. 5*A*). In this manner DnaK generates an unfolded state that resembles a water unfolded ensemble as far as secondary structure is concerned, but appearing more like a urea-unfolded ensemble from the standpoint of a lack of long-range transient tertiary interactions. Because the client protein released from DnaK begins folding from an initial conformation that structurally resembles the DnaK-bound state, our observations show that DnaK can strongly bias the starting conformation of substrates and thereby potentially influence the folding pathways adopted by client proteins en route to their native states (Fig. 5*A*).

On average, proteins contain approximately one DnaK binding site for every 40 amino acids of primary sequence (5), so that a 30-kDa protein (median size of proteins in *E. coli*) (53) is expected to have approximately seven DnaK binding sites. Thus, multiple DnaK molecules might bind a single client protein. Indeed, single molecule FRET data have been interpreted to suggest that five to six DnaK molecules bind denatured rhodanese (33 kDa) (12) before it folds to its native state. Because DnaK permits the formation of local secondary structure but not long-range tertiary contacts, at least in the context of hTRF1, the

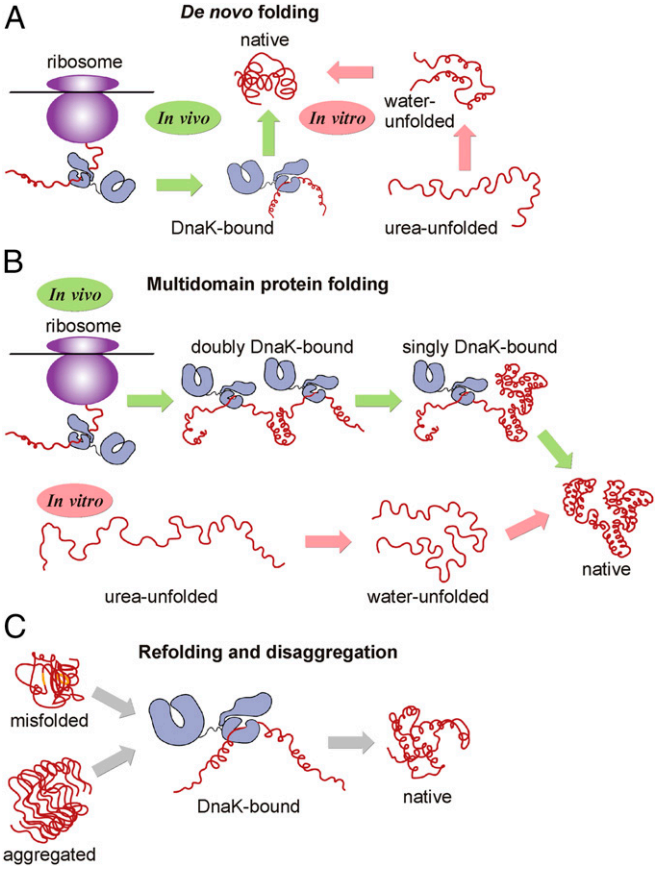

Fig. 5. A model for DnaK-dependent folding and disaggregation. (*A*) DnaK-bound hTRF1 has local secondary structure but lacks long-range tertiary interactions, unlike uw-hTRF1, which has contacts between helix 3 and helices 1 and 2. Consequently, folding pathways of client proteins from the DnaK-bound state in vivo may be different from in vitro refolding of the unfolded state present in water, as DnaK binding biases the energy landscape of the bound substrate. (*B*) The presence of multiple DnaK molecules on the client protein and their asynchronous release from the client allows local secondary and tertiary structure to develop before the establishment of long-range contacts. DnaK binding thus appears to favor a framework model for client folding, rather than a collapse-dependent nucleation-condensation mechanism. (*C*) The ability of DnaK to disrupt long-range contacts in the client substrate is of potential importance in the role that it plays in refolding, by converting misfolded substrates into a folding-competent conformation, and in disaggregation where DnaK unfolds the substrates and presents them to Hsp104/ClpB.

presence of regularly spaced DnaK molecules along the unfolded polypeptide suggests that DnaK may be able to alter the folding mechanism of clients in general to favor the formation of local structure before the establishment of long-range interactions (Fig. 5*B*). Moreover, because the bound DnaK molecules would be released stochastically and asynchronously, rather than all at once, formation of medium-range interactions between neighboring secondary structural elements would occur before the development of contacts between distal parts of the protein sequence that are separated by bound DnaK molecules (Fig. 5*B*). Taken together, our results indicate that the DnaK chaperone enables a protein chain to fold by establishing interactions in a distance dependent manner, via a process that can be likened to a framework-based diffusion collision mechanism rather than one in which collapse precedes acquisition of secondary structure through a nucleation-condensation model. These experimental results are similar to those obtained in a recent computational

Downloaded from https://www.pnas.org by UNIVERSITY OF MASSACHUSETTS on May 18, 2022 from IP address 128.119.52.1.

study in which the effect of the chaperonin GroEL/ES on protein folding was studied (54).

The ability of DnaK to disrupt transient long-range interactions may also be of relevance to the role played by Hsp70s in the refolding and disaggregation of client proteins. In contrast to native proteins, misfolded chains are generally not rigidly and stably packed but rather loosely structured with transient and often nonnative long-range contacts. Our data suggest that DnaK-binding can break long-range interactions in these misfolded ensembles and convert them into a globally unfolded state with only local secondary structure, thereby generating a conformation poised for folding to the native state on release from DnaK (Fig. 5*C*).

Materials and Methods

Sample Preparation. Labeling of hTRF1 with a nitroxide spin label was achieved by introducing a single Cys mutation at position 52 (K52C). $^{2}H/^{15}N$ K52C hTRF1 was overexpressed and purified using the same protocol as for WT hTRF1 (13) and stored in 5 mM DTT. Before labeling, pure K52C hTRF1 was buffer exchanged into degassed NMR buffer (50 mM Mes, pH 6.0, 50 mM KCl, 1 mM EDTA, 0.03% NaN_3), and concentrated to 1 mL. TEMPO-Mal spin label (Toronto Research Chemicals) was subsequently added in twofold molar excess and the labeling reaction allowed to occur at 4 °C overnight. The reaction was terminated by exchange into NMR buffer. All samples were submitted to MS analysis to ensure proper labeling. Reduced samples were generated through the direct addition of 100 mM ascorbic acid without or with 10 mM TCEP followed by buffer exchange into the NMR buffer. DnaK was overexpressed and purified as reported earlier (13). Urea-unfolded samples of K52C-tempol hTRF1 were prepared by unfolding native protein in NMR buffer containing 3.5 M urea for at least 30 min before data collection.

NMR Spectroscopy. NMR spectra were acquired at 35 °C on one of two 14.1 T (600 MHz) spectrometers, one of which was equipped with a cryogenically cooled probe. All experiments were carried out on the cold probe unless specified otherwise. Datasets were analyzed with NMRPipe (55) and visualized using NMRDraw (55) or Sparky (56).

CEST. CEST experiments were carried out using the pulse sequence shown in Fig. 2*A* and processed, analyzed, and fit as described in detail in *SI Text*.

^{1}H R_2. Amide proton transverse relaxation (^{1}H R_2) measurements were carried out using a previously described pulse sequence (35) on native K52C-tempol hTRF1, DnaK-bound K52C-tempol hTRF1, and urea-unfolded K52C-tempol hTRF1, with the spin labels in each case in either the oxidized or the reduced form. The native and urea-unfolded samples were prepared at K52C-tempol hTRF1 concentrations of 800 and 670 μM, respectively. The DnaK-bound sample contained 150 μM K52C-tempol hTRF1 and 300 μM DnaK, as well as 5 mM $MgCl_2$ and 5 mM ADP. Eight to 9 values of relaxation delays ranging between 6.7 and 25 ms were used for the DnaK-bound sample, 11 values between 6.7 and 40 ms were used for measuring ^{1}H R_2 rates of hTRF1 in water, and 10 delays from 6.7 to 35 ms were used for the urea-unfolded sample. ^{1}H R_2 experiments on K52C-tempol hTRF1 were carried out on a room temperature probe.

Peak intensities (I) as a function of relaxation delay (t) were determined by fitting individual lineshapes in 2D ^{1}H-^{15}N datasets using FuDA (pound.med.utoronto.ca/~flemming/fuda/) for native and urea-unfolded K52C-tempol hTRF1 or by determining the intensity at the peak center using Sparky for the DnaK-bound sample. In the latter case, peak centers were determined from the plane with the largest intensity and kept fixed for subsequent planes of the same dataset. Delay-dependent intensities were fit to a single exponential function of the form $I = I_0\exp(-R_2 t)$ to extract ^{1}H transverse relaxation rates (R_2). Errors in ^{1}H R_2 values were determined from the covariance matrix of the fit for native K52C-tempol hTRF1 and from three independent repeat experiments for DnaK-bound and urea-unfolded samples. PREs (Γ_2^{HN}) were calculated as the difference between ^{1}H R_2 values in the oxidized and reduced samples and errors in the PREs were estimated by propagating the errors in the R_2 measurements. Errors are reported as ±1 SD about the mean.

ACKNOWLEDGMENTS. This work was supported by grants from the Canadian Institutes of Health Research and the Natural Sciences and Engineering Research Council of Canada. L.E.K. holds a Canada Research Chair in Biochemistry.

1. Hartl FU, Bracher A, Hayer-Hartl M (2011) Molecular chaperones in protein folding and proteostasis. *Nature* 475(7356):324–332.
2. Mayer MP, Bukau B (2005) Hsp70 chaperones: Cellular functions and molecular mechanism. *Cell Mol Life Sci* 62(6):670–684.
3. Mayer MP (2013) Hsp70 chaperone dynamics and molecular mechanism. *Trends Biochem Sci* 38(10):507–514.
4. Clerico EM, Tilitsky JM, Meng W, Gierasch LM (2015) How Hsp70 molecular machines interact with their substrates to mediate diverse physiological functions. *J Mol Biol* 427(7):1575–1588.
5. Rüdiger S, Germeroth L, Schneider-Mergener J, Bukau B (1997) Substrate specificity of the DnaK chaperone determined by screening cellulose-bound peptide libraries. *EMBO J* 16(7):1501–1507.
6. Bertelsen EB, Chang L, Gestwicki JE, Zuiderweg ER (2009) Solution conformation of wild-type E. coli Hsp70 (DnaK) chaperone complexed with ADP and substrate. *Proc Natl Acad Sci USA* 106(21):8471–8476.
7. Kityk R, Kopp J, Sinning I, Mayer MP (2012) Structure and dynamics of the ATP-bound open conformation of Hsp70 chaperones. *Mol Cell* 48(6):863–874.
8. Qi R, et al. (2013) Allosteric opening of the polypeptide-binding site when an Hsp70 binds ATP. *Nat Struct Mol Biol* 20(7):900–907.
9. Palleros DR, Shi L, Reid KL, Fink AL (1994) hsp70-protein complexes. Complex stability and conformation of bound substrate protein. *J Biol Chem* 269(18):13107–13114.
10. Kurt N, Cavagnero S (2008) Nonnative helical motif in a chaperone-bound protein fragment. *Biophys J* 94(7):L48–L50.
11. Kurt N, Rajagopalan S, Cavagnero S (2006) Effect of hsp70 chaperone on the folding and misfolding of polypeptides modeling an elongating protein chain. *J Mol Biol* 355(4):809–820.
12. Kellner R, et al. (2014) Single-molecule spectroscopy reveals chaperone-mediated expansion of substrate protein. *Proc Natl Acad Sci USA* 111(37):13355–13360.
13. Sekhar A, Rosenzweig R, Bouvignies G, Kay LE (2015) Mapping the conformation of a client protein through the Hsp70 functional cycle. *Proc Natl Acad Sci USA* 112(33):10395–10400.
14. Sharma SK, De los Rios P, Christen P, Lustig A, Goloubinoff P (2010) The kinetic parameters and energy cost of the Hsp70 chaperone as a polypeptide unfoldase. *Nat Chem Biol* 6(12):914–920.
15. Winkler J, Tyedmers J, Bukau B, Mogk A (2012) Hsp70 targets Hsp100 chaperones to substrates for protein disaggregation and prion fragmentation. *J Cell Biol* 198(3):387–404.
16. Nishikawa T, Nagadoi A, Yoshimura S, Aimoto S, Nishimura Y (1998) Solution structure of the DNA-binding domain of human telomeric protein, hTRF1. *Structure* 6(8):1057–1065.
17. Gianni S, et al. (2003) Unifying features in protein-folding mechanisms. *Proc Natl Acad Sci USA* 100(23):13286–13291.
18. Vallurupalli P, Bouvignies G, Kay LE (2012) Studying "invisible" excited protein states in slow exchange with a major state conformation. *J Am Chem Soc* 134(19):8148–8161.
19. Vallurupalli P, Kay LE (2013) Probing slow chemical exchange at carbonyl sites in proteins by chemical exchange saturation transfer NMR spectroscopy. *Angew Chem Int Ed Engl* 52(15):4156–4159.
20. Long D, Sekhar A, Kay LE (2014) Triple resonance-based $^{13}C(\alpha)$ and $^{13}C(\beta)$ CEST experiments for studies of ms timescale dynamics in proteins. *J Biomol NMR* 60(4):203–208.
21. Wishart DS (2011) Interpreting protein chemical shift data. *Prog Nucl Magn Reson Spectrosc* 58(1-2):62–87.
22. Madl T, Bermel W, Zangger K (2009) Use of relaxation enhancements in a paramagnetic environment for the structure determination of proteins using NMR spectroscopy. *Angew Chem Int Ed Engl* 48(44):8259–8262.
23. Reckel S, et al. (2011) Solution NMR structure of proteorhodopsin. *Angew Chem Int Ed Engl* 50(50):11942–11946.
24. Xue Y, et al. (2009) Paramagnetic relaxation enhancements in unfolded proteins: Theory and application to drkN SH3 domain. *Protein Sci* 18(7):1401–1424.
25. Kristjansdottir S, et al. (2005) Formation of native and non-native interactions in ensembles of denatured ACBP molecules from paramagnetic relaxation enhancement studies. *J Mol Biol* 347(5):1053–1062.
26. Yao J, Chung J, Eliezer D, Wright PE, Dyson HJ (2001) NMR structural and dynamic characterization of the acid-unfolded state of apomyoglobin provides insights into the early events in protein folding. *Biochemistry* 40(12):3561–3571.
27. Gillespie JR, Shortle D (1997) Characterization of long-range structure in the denatured state of staphylococcal nuclease. I. Paramagnetic relaxation enhancement by nitroxide spin labels. *J Mol Biol* 268(1):158–169.
28. Mittag T, Forman-Kay JD (2007) Atomic-level characterization of disordered protein ensembles. *Curr Opin Struct Biol* 17(1):3–14.
29. Rosenzweig R, Moradi S, Zarrine-Afsar A, Glover JR, Kay LE (2013) Unraveling the mechanism of protein disaggregation through a ClpB-DnaK interaction. *Science* 339(6123):1080–1083.
30. Volkov AN, Worrall JA, Holtzmann E, Ubbink M (2006) Solution structure and dynamics of the complex between cytochrome c and cytochrome c peroxidase determined by paramagnetic NMR. *Proc Natl Acad Sci USA* 103(50):18945–18950.
31. Clore GM (2011) Exploring sparsely populated states of macromolecules by diamagnetic and paramagnetic NMR relaxation. *Protein Sci* 20(2):229–246.
32. McConnell HM (1958) Reaction rates by nuclear magnetic resonance. *J Chem Phys* 28(3):430–431.

Downloaded from https://www.pnas.org by UNIVERSITY OF MASSACHUSETTS on May 18, 2022 from IP address 128.119.52.1.

33. Bouvignies G, Kay LE (2012) Measurement of proton chemical shifts in invisible states of slowly exchanging protein systems by chemical exchange saturation transfer. *J Phys Chem B* 116(49):14311–14317.
34. Tadeo X, Castaño D, Millet O (2007) Anion modulation of the 1H/2H exchange rates in backbone amide protons monitored by NMR spectroscopy. *Protein Sci* 16(12): 2733–2740.
35. Donaldson LW, et al. (2001) Structural characterization of proteins with an attached ATCUN motif by paramagnetic relaxation enhancement NMR spectroscopy. *J Am Chem Soc* 123(40):9843–9847.
36. Schuler B, Eaton WA (2008) Protein folding studied by single-molecule FRET. *Curr Opin Struct Biol* 18(1):16–26.
37. Zhang O, Forman-Kay JD (1997) NMR studies of unfolded states of an SH3 domain in aqueous solution and denaturing conditions. *Biochemistry* 36(13):3959–3970.
38. Karplus M, Kuriyan J (2005) Molecular dynamics and protein function. *Proc Natl Acad Sci USA* 102(19):6679–6685.
39. Ishima R, Torchia DA (2000) Protein dynamics from NMR. *Nat Struct Biol* 7(9):740–743.
40. Carr HY, Purcell EM (1954) Effects of diffusion on free precession in nuclear magnetic resonance experiments. *Phys Rev* 94(3):630.
41. Meiboom S, Gill D (1958) Modified spin-echo method for measuring nuclear relaxation times. *Rev Sci Instrum* 29(8):688–691.
42. Palmer AG, 3rd, Kroenke CD, Loria JP (2001) Nuclear magnetic resonance methods for quantifying microsecond-to-millisecond motions in biological macromolecules. *Methods Enzymol* 339:204–238.
43. Nikolova EN, et al. (2011) Transient Hoogsteen base pairs in canonical duplex DNA. *Nature* 470(7335):498–502.
44. Fawzi NL, Ying J, Ghirlando R, Torchia DA, Clore GM (2011) Atomic-resolution dynamics on the surface of amyloid-β protofibrils probed by solution NMR. *Nature* 480(7376):268–272.
45. Forsén S, Hoffman RA (1963) Study of moderately rapid chemical exchange reactions by means of nuclear magnetic double resonance. *J Chem Phys* 39(11):2892–2901.
46. Sekhar A, Kay LE (2013) NMR paves the way for atomic level descriptions of sparsely populated, transiently formed biomolecular conformers. *Proc Natl Acad Sci USA* 110(32):12867–12874.
47. Hansen DF, Vallurupalli P, Lundström P, Neudecker P, Kay LE (2008) Probing chemical shifts of invisible states of proteins with relaxation dispersion NMR spectroscopy: How well can we do? *J Am Chem Soc* 130(8):2667–2675.
48. Vallurupalli P, Hansen DF, Kay LE (2008) Probing structure in invisible protein states with anisotropic NMR chemical shifts. *J Am Chem Soc* 130(9):2734–2735.
49. Vallurupalli P, Hansen DF, Stollar E, Meirovitch E, Kay LE (2007) Measurement of bond vector orientations in invisible excited states of proteins. *Proc Natl Acad Sci USA* 104(47):18473–18477.
50. Zhao B, Zhang Q (2015) Measuring residual dipolar couplings in excited conformational states of nucleic acids by CEST NMR spectroscopy. *J Am Chem Soc* 137(42): 13480–13483.
51. Long D, Bouvignies G, Kay LE (2014) Measuring hydrogen exchange rates in invisible protein excited states. *Proc Natl Acad Sci USA* 111(24):8820–8825.
52. Peng JW, Wagner G (1992) Mapping of spectral density functions using heteronuclear NMR relaxation measurements. *J Magn Reson* 98(2):308–332.
53. Skovgaard M, Jensen LJ, Brunak S, Ussery D, Krogh A (2001) On the total number of genes and their length distribution in complete microbial genomes. *Trends Genet* 17(8):425–428.
54. Kmiecik S, Kolinski A (2011) Simulation of chaperonin effect on protein folding: A shift from nucleation-condensation to framework mechanism. *J Am Chem Soc* 133(26):10283–10289.
55. Delaglio F, et al. (1995) NMRPipe: A multidimensional spectral processing system based on UNIX pipes. *J Biomol NMR* 6(3):277–293.
56. Goddard T, Kneller D (2006) *Sparky—NMR Assignment and Integration Software* (Univ of California, San Francisco).
57. Levitt MH (1986) Composite pulses. *Prog Nucl Magn Reson Spectrosc* 18(2):61–122.
58. Marsh JA, Singh VK, Jia Z, Forman-Kay JD (2006) Sensitivity of secondary structure propensities to sequence differences between α- and γ-synuclein: Implications for fibrillation. *Protein Sci* 15(12):2795–2804.
59. McCoy M, Mueller L (1993) Selective decoupling. *J Magn Reson* 101(2):122–130.
60. Morris GA, Freeman R (1979) Enhancement of nuclear magnetic resonance signals by polarization transfer. *J Am Chem Soc* 101(3):760–762.
61. Taylor J (1997) *Introduction to Error Analysis: The Study of Uncertainties in Physical Measurements* (University Science Books, Herndon, VA).
62. Efron B, Tibshirani R (1986) Bootstrap methods for standard errors, confidence intervals, and other measures of statistical accuracy. *Stat Sci* 1(1):54–75.
63. Cavanagh J, Fairbrother WJ, Palmer AG, Skelton NJ (1995) *Protein NMR spectroscopy: Principles and Practice* (Academic Press, New York).
64. Tjandra N, Bax A (1997) Solution NMR measurement of amide proton chemical shift anisotropy in 15N-enriched proteins. Correlation with hydrogen bond length §. *J Am Chem Soc* 119(34):8076–8082.
65. Yao L, Grishaev A, Cornilescu G, Bax A (2010) The impact of hydrogen bonding on amide 1H chemical shift anisotropy studied by cross-correlated relaxation and liquid crystal NMR spectroscopy. *J Am Chem Soc* 132(31):10866–10875.
66. Sattler M, Schleucher J, Griesinger C (1999) Heteronuclear multidimensional NMR experiments for the structure determination of proteins in solution employing pulsed field gradients. *Prog Nucl Magn Reson Spectrosc* 34(2):93–158.

Downloaded from https://www.pnas.org by UNIVERSITY OF MASSACHUSETTS on May 18, 2022 from IP address 128.119.52.1.